Microstructure and texture development during hot-compression of Ti5321

Gu, B.; Chekhonin, P.; Xin, S. W.; Liu, G. Q.; Ma, C. L.; Zhou, L.; Skrotzki, W.;

Microstructure and texture development during hot-compression of Ti5321

B. Gu[1,2,∗] , P. Chekhonin[3], S.W. Xin[4], G. Q. Liu[5], C.L. Ma[1, ∗], L. Zhou[1,4], W. Skrotzki[2]

[1] Key Laboratory of Aerospace Advanced Materials and Performance of Ministry of Education, School of Materials Science and Engineering, Beihang University, Beijing 100191, China

[2] Institute of Solid State and Materials Physics, Dresden University of Technology, 01062 Dresden, Germany

[3] Helmholtz-Zentrum Dresden-Rossendorf, 01328 Dresden, Germany

[4] Northwest Institute for Nonferrous Metal Research, Xi'an 710016, China

[5] School of Mechanical Engineering and Automation, Beihang University, Beijing 100191, China

Abstract

The microstructure and texture development of the metastable β-titanium alloy Ti5321 during hot-compression were investigated by electron backscatter diffraction. Above the β-transus temperature, deformation is accompanied by continuous dynamic recrystallization leading to immediate steady state flow. The deformation below the β-transus temperature is significantly affected by α-precipitation. Dynamic globularization of the α-lamellae leads to flow softening. During hot-compression, parallel to the compression axis a <100> <111> double fiber texture develops. With increasing temperature the intensity of <100> increases, while that of <111> decreases. At all temperatures <100> is dominant.

[∗] Corresponding author:

 E-mail: gubin_buaa@hotmail.com (B.Gu)

[∗] Corresponding author:

 E-mail: machaoli@buaa.edu.cn (C.L. Ma)

Keywords: Metastable β-titanium alloy, hot-compression, texture, dynamic recovery, dynamic recrystallization, precipitation

1. Introduction

Metastable body-centered cubic (bcc) β-titanium alloys because of their good workability, high strength-to-density ratio and good fatigue properties are commonly used as materials in aircraft applications [1]. These alloys are generally sensitive to processing. Hence, changing the processing parameters may result in different microstructures, textures and properties. Consequently, in order to optimize the processing routes and control the evolution of microstructure and texture of metastable β-Ti alloys, it is necessary to study the relationship of processing parameters and deformation behavior.

Lütjering and Williams stated that thermomechanical processing (TMP) of metastable β-Ti alloys involves deformation in the ($\alpha+\beta$)- or β-phase field [1]. Most of the publications reported that dynamic recovery (DRV) is the dominant restoration mechanism in the β-phase field with an apparent activation energy close to that of Ti-diffusion in β-Ti alloys [2-4]. During deformation above the β-transus temperature (T_β), frequently dynamic recrystallization (DRX) was observed [3-6]. DRX can be classified into discontinuous dynamic recrystallization (DDRX) and continuous dynamic recrystallization (CDRX) [7-10].

In conventional DDRX, during deformation the formation of new grains involves the process of nucleation and growth. The mechanism of CDRX is quite different. Here, new grains form by incorporation of deformation-induced dislocations into subgrain boundaries (low angle grain boundaries, LAGBs) by this increasing their misorientation and changing

them to high angle grain boundaries (HAGBs) [3, 6, 8, 11, 12]. Geometric dynamic recrystallization (GDRX) is considered as another kind of CDRX [13], but it takes place at high temperatures. When grain boundary bulges become comparable with the thickness of elongated/flattened grains, the process of grain impingement occurs by interpenetrating of the scalloped boundaries. There have been several studies on DRX during hot-compression of Ti alloys above T_β. CDRX was reported in the vicinity of α/β phase boundaries in Ti5553 samples deformed at strain rates of 10^{-3} s^{-1} and 10^{-2} s^{-1} [6]. Zhao et al. [3] have revealed CDRX in Ti1023 by progressive lattice rotation occurring at high strain rates and low temperatures (high Zener-Hollomon parameter). Dikovits et al. [14] found GDRX and CDRX during hot-deformation of Ti55531, too. Although during TMP different kinds of DRX were observed by many researchers, the influence of strain and temperature on different types of DRX still lacks systematic and quantitative analysis.

Moreover, DRV and DRX affect texture formation，which may lead to inhomogeneous recrystallization [13]. Many researchers have investigated different modes of deformation such as sheet rolling processes and shape rolling [15-19]. However, systematic investigations on mechanisms of deformation and texture evolution during hot-compression are limited.

During hot-deformation of metastable β-Ti alloys below T_β, flow behavior and DRX mechanisms can be affected by intervening metallurgical reactions such as precipitation or phase transformation [7]. Warchomicka et al. [4] found that GDRX takes place in Ti55531 at large strains due to pinning of dislocations by α-precipitates. Flow softening behavior below T_β has been observed in other β-Ti alloys such as Ti5553, Ti55531, Ti1023, Ti7333 and Ti1033 [6, 4, 20, 21, 22]. It was attributed to inhomogeneous deformation (flow instability)

[4, 21] and the influence of dynamic α-precipitation [6, 20]. However, research on the relationship between DRX, flow softening and phase transformation remains limited.

Thus, it is the aim of this study to analyze the effect of strain and temperature on the deformation mechanisms in Ti5321, especially regarding DRX and flow softening. Based on the previous study [19, 23], the recently developed metastable β-Ti alloy Ti5321 at room temperature (RT) is characterized by an ultimate tensile strength of 1238 MPa, elongation to fracture of 20% and fracture toughness of 73 MPa·m$^{1/2}$. The results can be used to optimize the TMP parameters of metastable β-Ti alloys.

In the following, it is appropriate to present the results and the discussion by crossing T_β from high to low temperature, i.e. from the single to the two phase temperature region.

2. Experimental

The metastable β-Ti alloy Ti5321 used has the composition Ti-5.02Al-3.03Mo-2.99V-2.06Cr-2.01Zr-1.37Nb-0.99Fe-0.004N-0.0011H-0.064O (wt.%) [19, 23]. T_β of the alloy measured by metallographic method is (855 ± 5)°C [19, 23]. The alloy was bar-rolled in the $(\alpha+\beta)$-phase field to a diameter of 20 mm. Before the compression tests the samples were annealed at 900°C for 1h and then quenched in water (further referred to as ST state).

Cylindrical samples of 8 mm diameter and 12 mm length were hot-compressed in vacuum in a Gleeble-3800 machine. In order to minimize friction, top and bottom sides of the samples were mechanically grinded. The thermocouple was located at mid-height of the samples. In order to further reduce friction and keep the deformation uniform, thin tantalum

sheets were placed between compression specimen and dies. The samples were compressed to high engineering strains of 40%, 60%, 80% (absolute values, in the following just called strains) at temperatures of 750°C, 800°C, 830°C, 900°C and 950°C at an initial strain rate of $10^{-2}\,s^{-1}$. The engineering strain was controlled during hot-compression by stroke displacement control mode through controlling the displacement of the anvil. For testing temperatures below T_β, the samples were heat treated for 2 min at the corresponding test temperature before compression so as to ensure homogeneous temperature distribution within the sample and increase the volume fraction of lamellar α (hexagonal phase). After compression the samples were water-quenched. One sample was tested per condition.

The microstructure and texture was investigated through backscatter electron (BSE) imaging and electron backscatter diffraction (EBSD) in a ZEISS ULTRA 55 scanning electron microscope (SEM). Data acquisition and analysis were done by a Nordlys HKL EBSD system with Channel 5 software. The samples for SEM were mechanically grinded using wet SiC-paper (final step: 4000 grid) and then electropolished in a solution of one part perchloric acid (70 vol.%) and nine parts of ethanol using a voltage of 40 V for 40 s while keeping the electrolyte at –14°C. The range of accelerating voltage for EBSD mappings was 10-20 kV. For large areas (about 4 mm^2), the scanning step size was 3 μm, whereas for small areas (about 400 μm^2), it was 80 nm. The grain size was determined by the line intercept method of HKL Channel 5 EBSD software. Pole figures (PFs) and inverse pole figures (IPFs) were calculated from the EBSD data. The IPF maps taken in the central portion of the samples show orientations with respect to the compression axis (CA), abbreviated as IPF-CA. To ensure acceptable statistics in each pole figure, at least two EBSD maps were taken

including more than 1000 grains in sum. The volume fractions of texture fibers (15°

orientation spread) were calculated using HKL Channel 5 EBSD software. The texture of the

β-phase below T_β was determined by removing the α-phase orientation data.

Wright et al. [24] stated that the recrystallized grains can be determined through the

grain orientation spread (GOS) defining the average deviation in orientation between each

point in a grain and the average orientation of the grain. A grain will be taken as

recrystallized for GOS less than 2° [25, 26].

3. Results

3.1. Flow behavior

The true stress – true strain curves for temperatures between 750°C and 950°C are shown

in Fig. 1. The overall magnitude of the flow stress decreases with increasing temperature.

While above T_β (855°C) after a few percent of strain a steady state flow stress is reached,

below T_β the flow curves are characterized by a short strain hardening region, a well-defined

peak stress and then remarkable flow softening. The magnitude of flow softening estimated

by $(\sigma_P - \sigma_l)/\sigma_P$ (σ_P = peak stress, σ_l = lower stress at a true strain of about 0.8) amounts 114

MPa/202 MPa = 56%, 50 MPa/110 MPa = 45% and 5 MPa/54 MPa = 9% for samples tested

at 750°C, 800°C and 830°C, respectively. At strains larger than about 0.8 the stress slightly

increases because at such strain levels the "dead metal zones" get in contact [27]. Therefore,

this effect may be regarded as an artifact of large-strain compression. There is an exception

for the curve at 750°C, where above a true strain of about 1.0 the stress decreases again. This

effect will be discussed below.
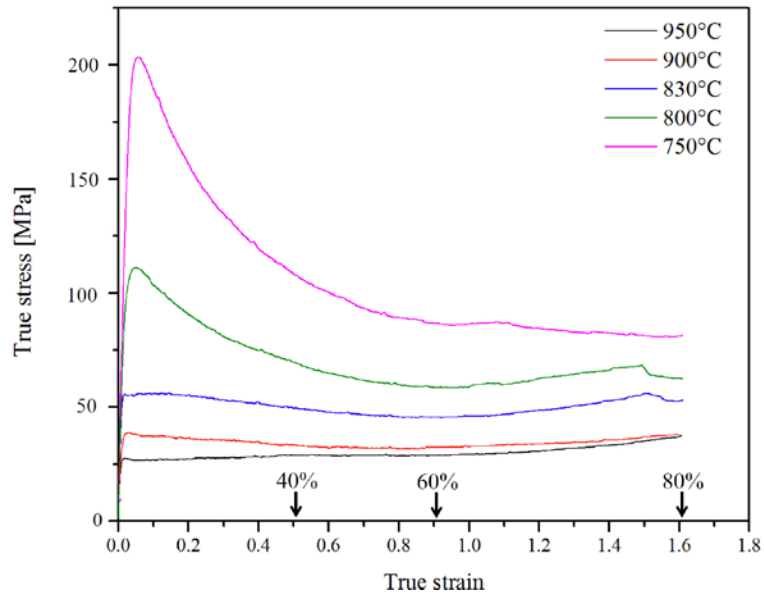
Fig. 1: True stress – true strain curves of Ti5321 hot-compressed at temperatures between 750°C and 950°C. Engineering strains of 40%, 60% and 80% are marked by arrows.

3.2. Microstructure

The microstructure of the as-received Ti5321 bar is presented in Fig. 2a. The bar was heated at 900°C for 1h and then water-quenched to RT (Fig. 2b). After annealing the grains are equiaxed with an average size of 165 µm. The texture acquired as a combination of three EBSD maps (like Fig. 2b) including about 450 grains is almost random, as shown by the {100} and {111} PFs in Fig. 2c.
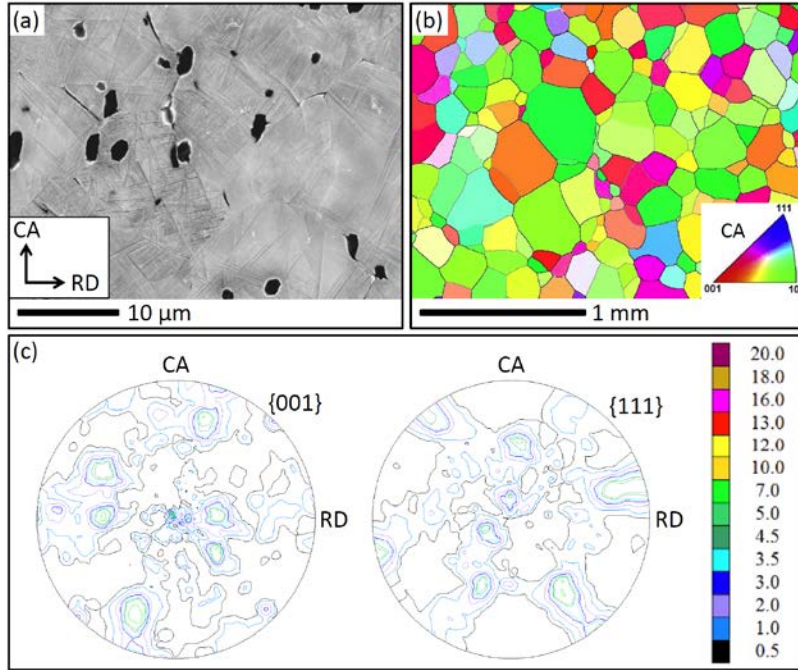
Fig. 2: (a) SEM BSE micrograph of the as-received material with the β-phase bright and the α-phase dark (CA = compression axis, RD = radial direction). (b) EBSD IPF-CA map in the CA-RD plane showing the microstructure of the ST state. (c) {100} and {111} PFs of the β-phase in the ST state (intensities are given in mrd = multiples of a random distribution).

Figure 3 shows the EBSD IPF-CA maps of samples compressed to strains of 40%, 60% and 80% between 750°C and 950°C. To provide details on the microstructure after hot-compression, grain boundary maps of representative samples are shown in Fig. 4 (rectangular subsets in Figs. 3a - c, g - i). Deformation parameters such as strain and temperature have significant influence on the microstructure development during hot-compression. The change of morphology and orientation of the grains from 750°C to 950°C (Figs. 3 and 4) is evident in comparison to the initial microstructure (Fig. 2b). At all deformation temperatures with increasing strain the initially equiaxed grains get flattened (Fig. 3). In the rim of the grains a subgrain structure develops with the subgrain size

increasing with deformation temperature (Fig 4). Moreover, with increasing deformation temperature and strain fine new grains are formed in the rim (Figs. 3a and 4a). At any given deformation temperature, the majority of β-grains is oriented with their <100> axis close to CA (red color). With decreasing deformation temperature and with lower strain, this preference appears to be reduced. After 40% deformation below T_β (Figs. 3j and m) the grain boundaries are nearly straight and within the limit of resolution no recrystallized grains are observed.
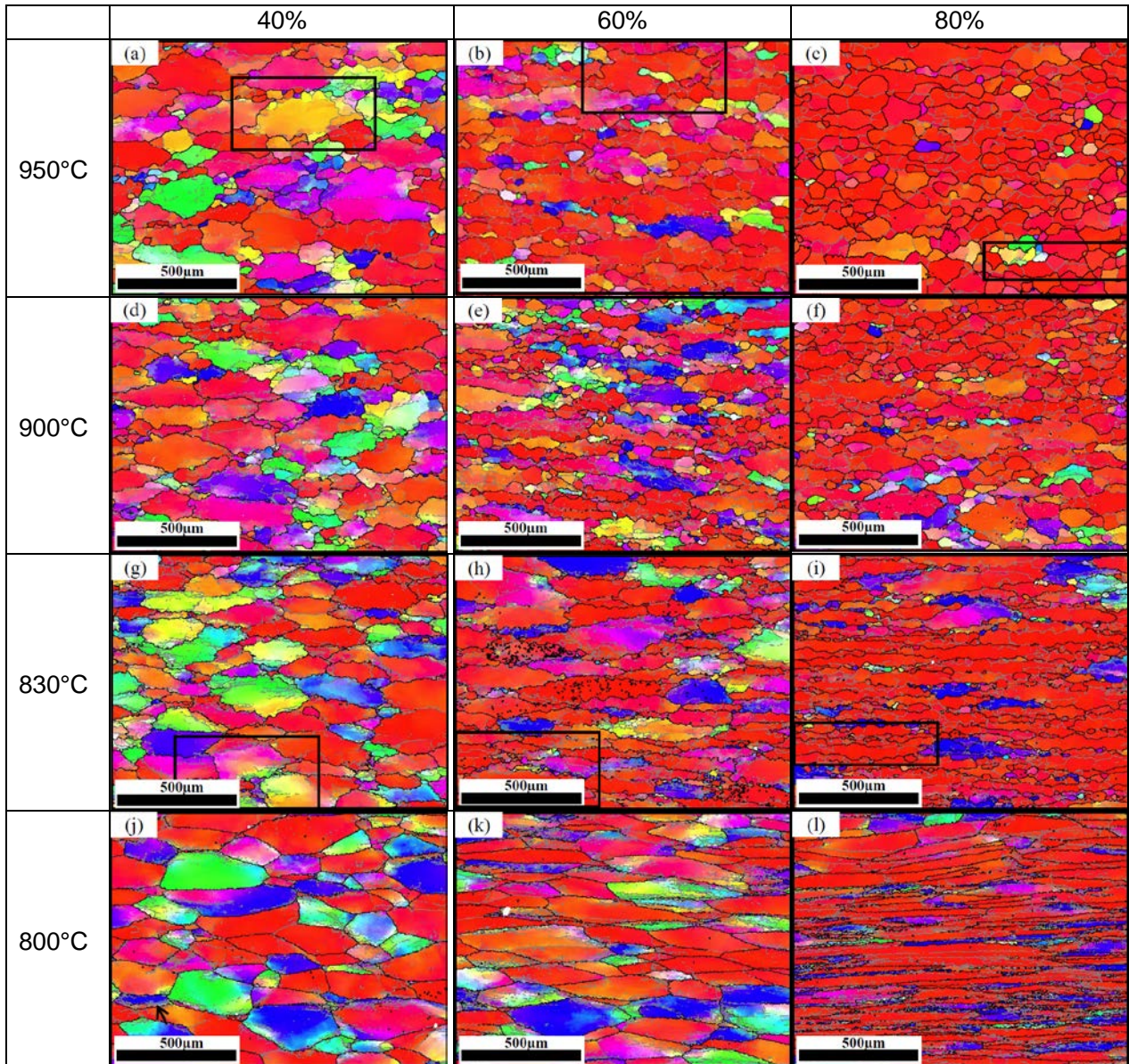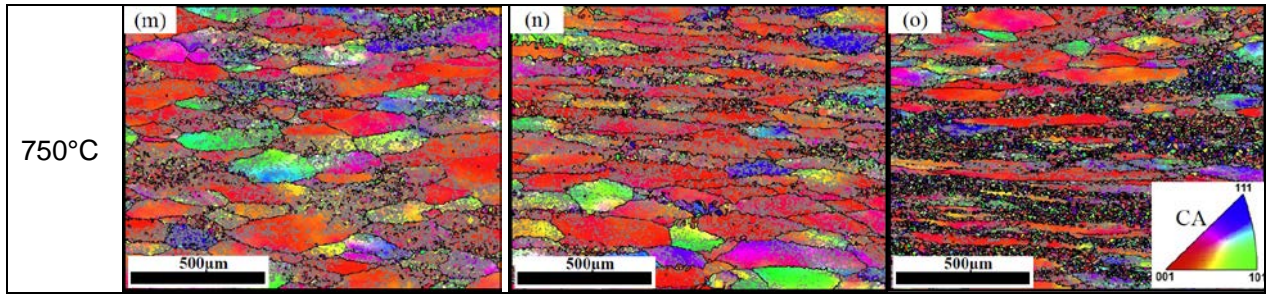
Fig. 3: EBSD IPF-CA maps of the *β*-phase in the Ti5321 alloy following hot-compression to strains of 40%, 60% and 80% at different temperatures. (gray lines: LAGBs with misorientation between 3° and 15°, black lines: HAGBs, misorientation greater than 15°) Detailed grain boundary maps of rectangular areas in (a-c) and (g-i) are given in Fig. 4. (sample reference system as in Fig. 2a)
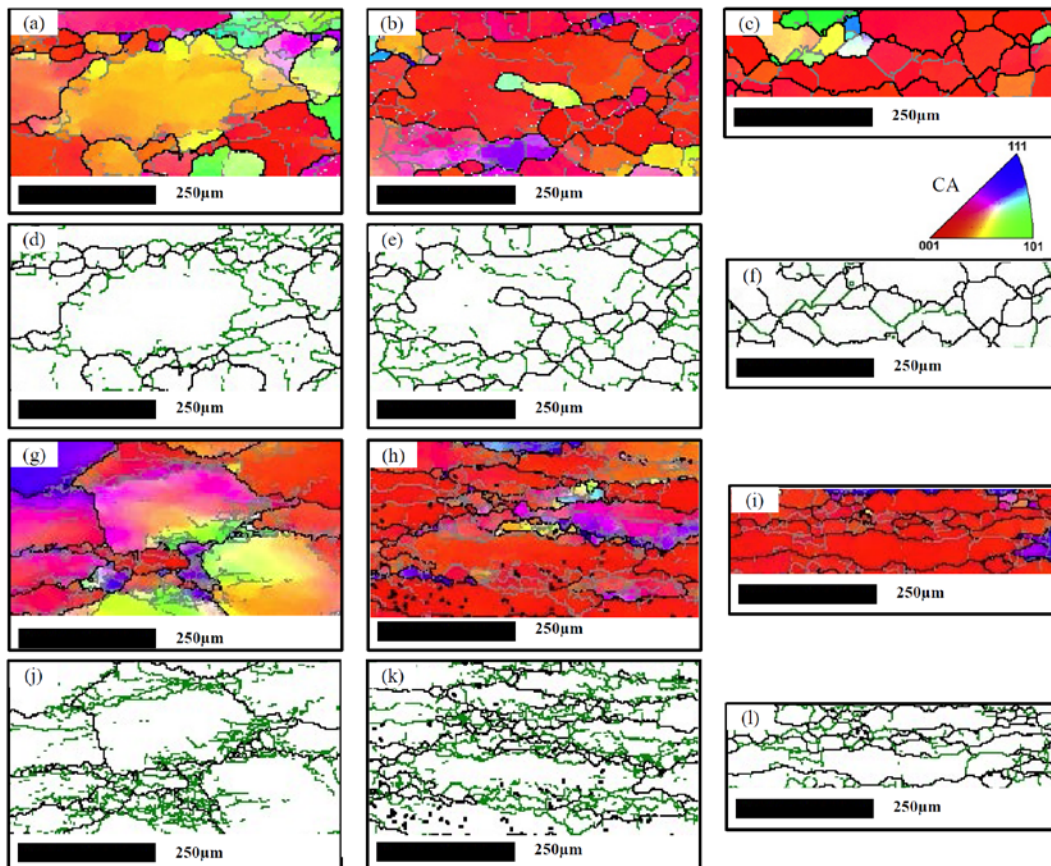

Fig. 4: EBSD orientation maps (LAGBs in grey and HAGBs in black) of rectangular areas in

10

Figs. 3a - c and corresponding grain boundary maps of samples hot-compressed at 950°C to strains of 40% (a and d), 60% (b and e) and 80% (c and f); grain boundary maps of rectangular areas in Figs. 3g - i of samples hot-compressed at 830°C to strains of 40% (g and j), 60% (h and k) and 80% (i and l). (green lines: LAGBs, black lines: HAGBs, sample reference system as in Fig. 2a)

With increasing strain, the β-grains become flattened perpendicular to CA, their average aspect ratio $R = a/c$ (a = semi-major axis, c = semi-minor axis, of the rotational ellipsoidal grains) is given in Fig. 5. Assuming that before deformation the β-grains are spheres with radius r (compare Fig. 2b), then the geometrical aspect ratio R_g is that of the grains solely geometrically deformed without any change by DRX. As during axisymmetric compressive deformation the volume of the grains remains the same, $4/3\pi r^3 = 4/3\pi a^2 c$ (r = radius before deformation), with $\varepsilon = (r\text{-}c)/r$, R_g is given by $R_g = \sqrt{\dfrac{1}{(1-\varepsilon)^3}}$.

Because of the low volume fraction of recrystallized grains after strains of 40% and 60%, the aspect ratio does not differ much from the geometrical one (Fig. 5). However, after a strain of 80% for any given temperature the aspect ratio is below the geometrical value. Grain aspect ratios of the samples hot-compressed at 900°C and 950°C are lowest indicating a higher volume fraction of DRX grains.
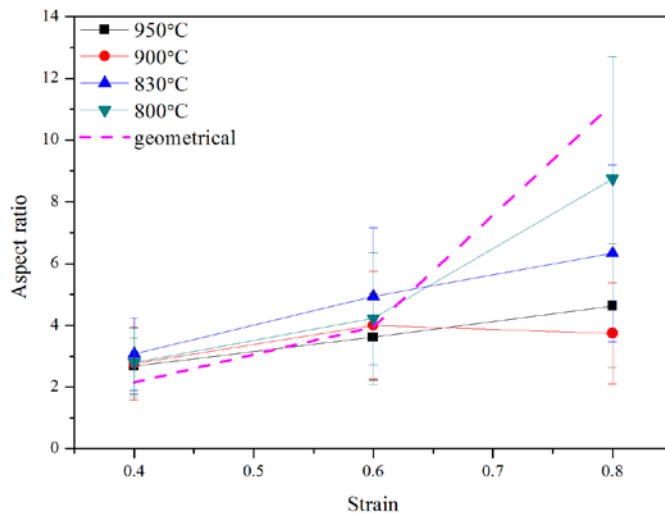
**Fig. 5:** Average *β*-grain aspect ratio as a function of strain for compression at different temperatures.

It has been reported that internal misorientation within grains can be attributed to the strain distribution and stored energy [24, 25, 28]. Enhanced values of GOS indicate a comparably high dislocation density and stored energy inside the material, while in contrast a recrystallized sample with a low dislocation density will typically exhibit a comparatively low GOS value. As a result, using GOS the microstructure can be separated into deformed and recrystallized areas. In this work a grain is classified as recrystallized if its GOS is below $2°$ [24-26].

The relationship between strain and volume fraction of dynamically recrystallized grains is given in Fig. 6. It distinctly rises with increasing strain and deformation temperature. Because of the low indexation rate (about 50%) of samples compressed at 750°C (Figs. 3m – o), the volume fraction and size of recrystallized grains could not be determined in this study. At the highest strain at 800°C and 950°C, the fraction of recrystallized grains is 0.04 and 0.26,

respectively. The relationship between strain and recrystallized grain size is given in Fig. 7.
Because of the low indexation rate of samples compressed at 750°C and the very low volume
fraction of recrystallized grains in samples compressed at 800°C (Fig. 6), only the size of
recrystallized grains in samples deformed at 830°C, 900°C and 950°C is presented. The size
of dynamically recrystallized grains increases moderately with strain, but stronger with
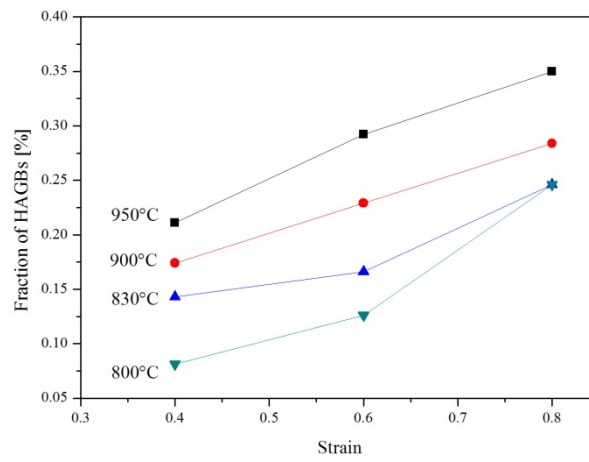deformation temperature (Fig. 7).
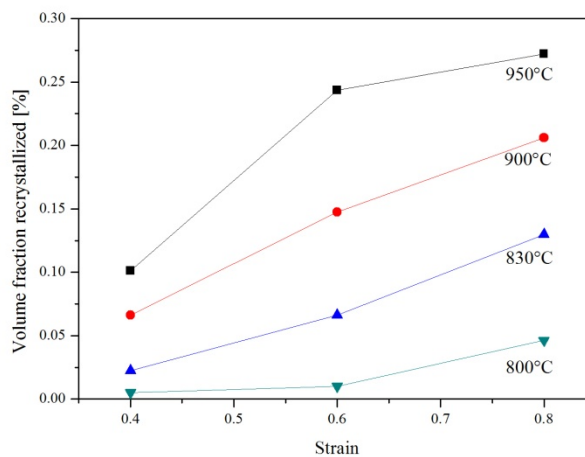
Fig. 6: Volume fraction of dynamically recrystallized grains as a function of strain for compression at different temperatures.
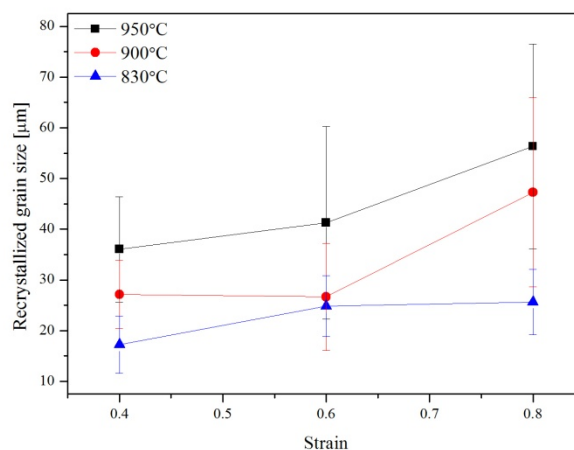

Fig. 7: Recrystallized grain size as a function of strain for compression at different temperatures.

Due to subgrain formation during straining the fraction of HAGBs from an intial value of about 80%, typical for a fully recrystallized grain structure (Fig. 2b), first decreases due to subgrain formation and then increases again when new grains are formed by DRX (Fig. 8). The fraction of HAGBs increases with deformation temperature, i.e. with increasing subgrain size and more intense DRX.

Fig. 8: Fraction of HAGBs as a function of strain for compression at different temperatures.

In the samples deformed below T_β the volume fraction of recrystallized grains is lower than in samples deformed above (Fig. 6). Figure 9 presents the microstructure evolution of samples deformed to different strains at 750°C and 800°C. The volume fraction of the α-phase is lower at 750°C than that at 800°C, as shown for a strain of 80% (compare Figs. 9f and h). It seems to slightly increase with strain. The α-phase exists in the grain interior as well as at grain boundaries and triple junctions. At 750°C few fine β-subgrains/grains (~ 1 μm) have formed in the rim of original β-grains. There are no fine β-grains observed at 800°C.
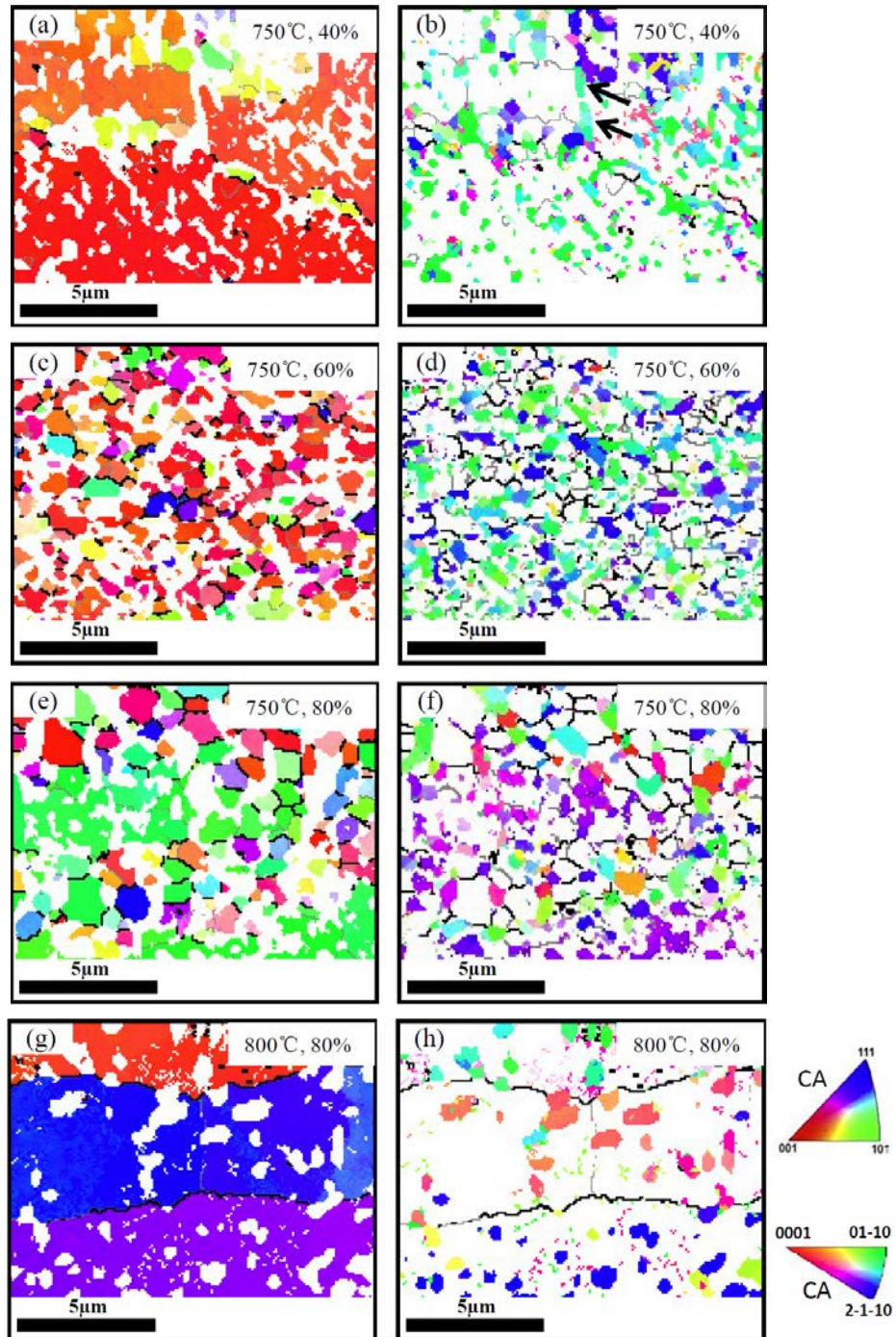
Fig. 9: EBSD IPF-CA maps (CA–RD plane) of samples compressed at 750°C up to strains of 40% (a and b), 60% (c and b) and 80% (e and f), and at 800°C up to strains of 80% (g and h). In IPFs a, c, e and g only the β-phase is shown in color, while in IPFs b, d, f and h it is only the α-phase (gray lines: LAGBs, black lines: HAGBs of β-phase). In (b) α-phase along β HAGBs is marked by black arrows.

Figure 10 shows the average aspect ratio and size (area) of α-grains in samples hot-compressed to different strains at 750°C and 800°C. At constant compression temperature, the size of α-grains slightly increases with strain, whereas the aspect ratio slightly decreases.
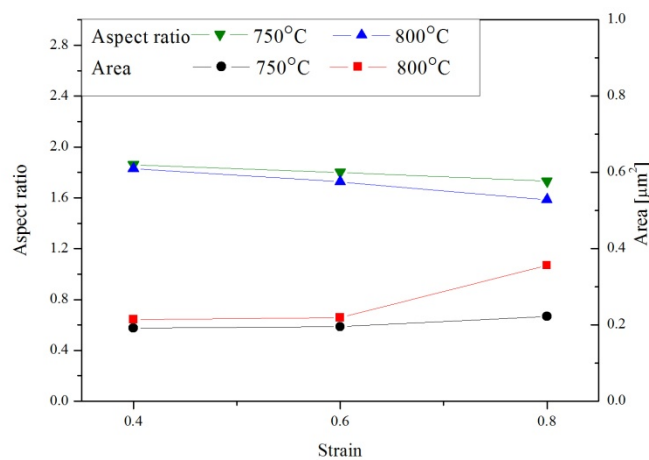

Fig. 10: Average aspect ratio and size (area) of α-grains in samples deformed at 750°C and 800°C to different strains.

3.3. Texture

Due to axisymmetric compression in the bcc β-phase a <100> <111> double fiber texture with the fiber axes parallel to CA developed. The {100} PFs of Fig. 11 clearly show that the preferred fiber axis for all compression temperatures and strains is <100>. A quantitative analysis of the volume fraction of the <100> fiber reveals that at constant temperature there is an obvious increase with strain, while at constant strain there is no strict increase with temperature (Figs. 12a and b). At constant temperature below T_β the volume fraction of the <111> fiber slightly increases with strain, whereas above T_β it slightly decreases. At constant

strain the <111> fiber decreases with temperature (Figs. 12c and d).
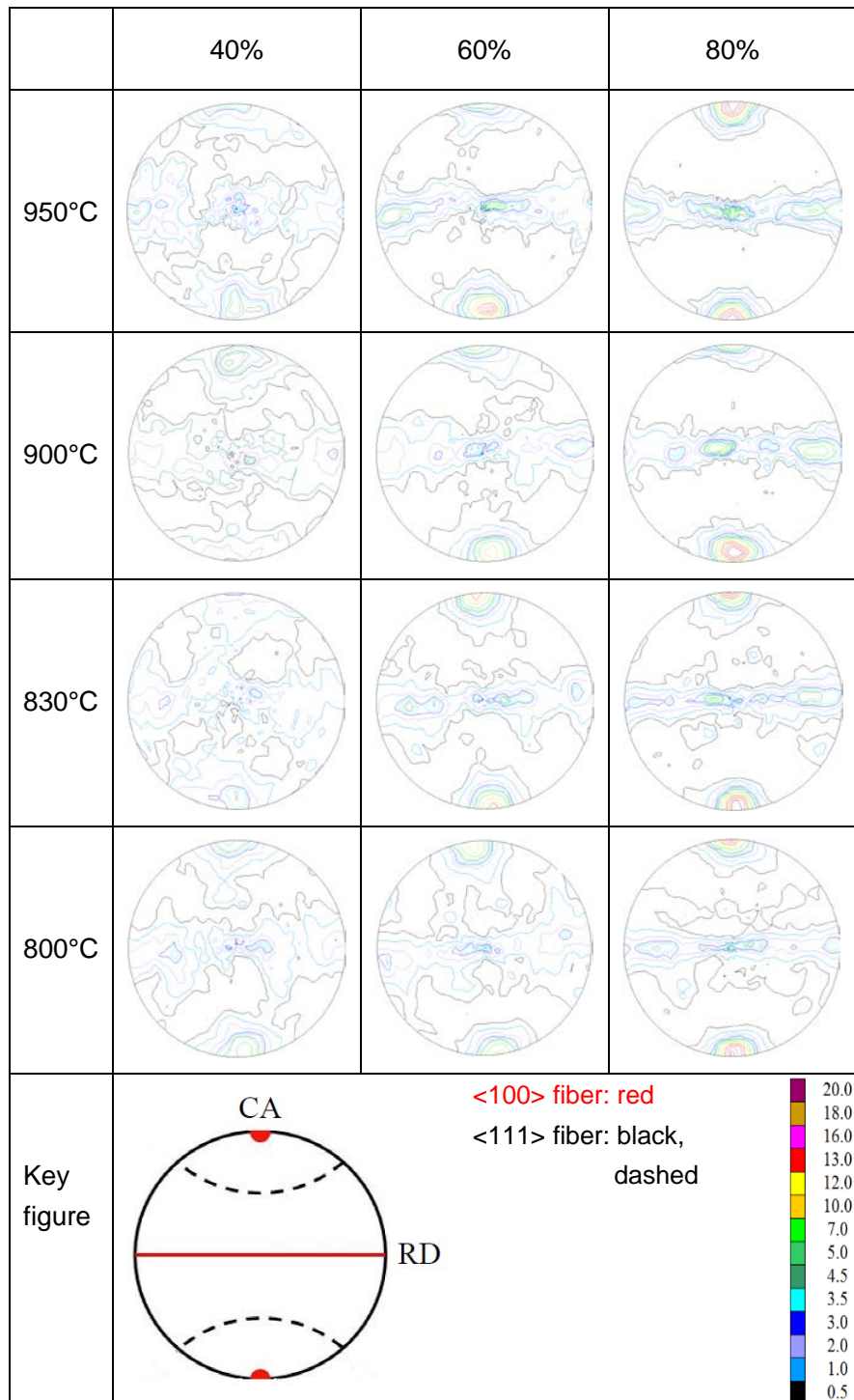
Fig. 11: {100} PFs of the *β*-phase in Ti5321 alloy following compression to strains of 40%, 60% and 80% at temperatures between 800°C and 950°C (intensities are given in mrd).
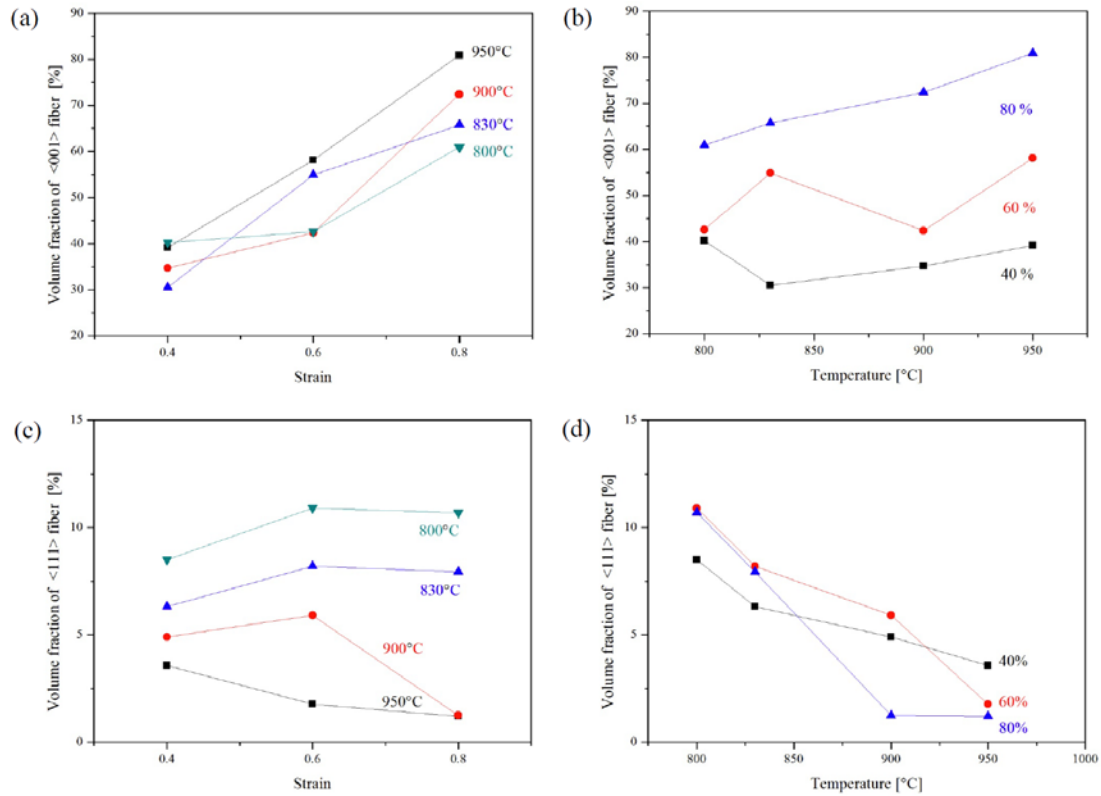
Fig. 12: Volume fraction of <100> fiber (a and b) and <111> fiber (c and d) of the *β*-phase as a function of strain for compression at different temperatures, and temperature at different strains.

4. Discussion

4.1. Microstructure evolution

The microstructure evolution during hot-deformation of Ti5321 is characterized by CDRX, which is based on extended DRV. During deformation lattice rotation within an individual grain is impeded near the grain boundaries by the constraining effects of neighboring grains giving rise to lattice curvature [29]. This lattice curvature in the rim of grains is accommodated by geometrically necessary dislocations which due to DRV may arrange themselves into LAGBs. With increasing strain more and more dislocations are incorporated

into the LAGBs by this increasing their misorientation. Finally, this results in the transformation of LAGBs into HAGBs, i.e. there is a change from a subgrain to a grain structure. With increasing strain this process extends to the grain interior, the faster the higher the deformation temperature. During hot-deformation, the applied stress provides an additional force for stress-assisted migration of LAGBs. This migration may lead to annihilation of opposing boundaries (subgrain coalescence) and movement of triple junctions, so that subgrains remain almost equiaxed. As grain boundary and triple junction movement are diffusion-controlled, subgrain/grain size increases with temperature. Moderate grain coarsening and renewed subdivision due to deformation leads to a steady state grain structure (Figs. 3c and f). The orientation of the new DRX grains is mainly determined by deformation. However, as the HAGBs at high temperature get mobile there is a driving force for bulging into grains with a higher dislocation/subgrain density, such as grains with orientations deviating from <100>, in particular those with <111> orientation having the highest Taylor factor (Figs. 3 and 4) [30]. As a consequence, with increasing strain and temperature the intensity of the <100> fiber increases on the cost of <111>.

Below T_β the volume fraction recrystallized is lower than in samples compressed above. Moreover, the subgrain and recrystallized grain size is lower. On the one hand this is due to lower deformation temperature, respectively higher flow stress, on the other hand a dual phase $\alpha+\beta$ microstructure exists which during straining changes from lamellar to globular (dynamic globularization). The second phase particles impede dislocation motion and hence increase the dislocation density, which promotes the formation of CDRX β-grains. Because α-precipitates also inhibit the movement of β-subgrain boundaries, the subgrain size is

limited by the precipitate spacing. With increasing strain the LAGBs are transformed to HAGBs. The resulting β-grain structure after high strains at 750°C is very fine-grained, in the order of 1 μm (Fig. 9). CDRX at this temperature at a true strain larger than about 1.0 leads to flow softening, which may be due to grain/interphase boundary sliding (Fig. 1). This softening effect is much less than that induced by dynamic globularization at smaller strains (see section 4.3).

4.2. Texture evolution

Generally, β-Ti alloys are sensitive to processing parameters because of the fact that the β-phase (bcc structure) has more easy to activate independent slip systems than the α-phase (hcp structure). Moreover, the β-phase represents a relatively high volume fraction during thermomechanical treatment. Thus, the detailed microstructural investigation, including orientation changes due to DRV and CDRX, provides an interesting case to study the effects of DRV and DRX on texture evolution. This may complement the understanding of the microstructural evolution in the β-phase.

The axisymmetric texture developed during hot-compression is a <100> <111> double-fiber texture with <100> fiber dominating. Similar observations were reported for Ti-5Al-5Mo-5V-1Cr-1Fe (Ti55511) [25] and other bcc materials [31, 32]. The <100> <111> double-fiber texture was forecasted as stable texture after compressive deformation by Barrett et al. [33] based on the theories that three most stressed slip systems ({110}<111>, {112}<111> or {123}<111>) are activated in bcc structures. Moreover, it was reported that slip systems {112}<111> and {123}<111>, both lead to <100> and <111> fiber textures, whereas the {110}<111> slip system leads to a strong <111> fiber. Thus, the strengthening of

the <100> fiber and weakening of the <111> fiber with temperature may be attributed to the higher slip activity on {112} and {123} due to facilitated cross slip [34]. Another reason may be the bulging of HAGBs into grains with higher dislocation/subgrain density as already mentioned in section 4.1.

With decreasing deformation temperature below T_β the volume fraction of precipitated α-phase increases. Texture development of the β-phase is affected by the volume fraction, size and distribution of the harder α-grains. In general, in two-phase materials texture strength decreases with increasing volume fraction of secondary phase. To study the texture development below T_β in more detail, neutron texture measurements of both phases are in progress.

4.3. Flow softening

The stress - strain curves follow two different trends indicating different deformation mechanisms at different compression temperatures (Fig. 1). The flow curves above T_β are similar to those found in Ti55531, Ti5553 and Ti1023 [3, 4, 6]. In the present study, above T_β the flow stress with strain quickly rises to a steady state. This is characteristic of a material where during deformation extensive recovery takes place by non-conservative movement of dislocations balancing work-hardening [8, 13]. Moreover, it has been previously reported that DRV is the dominant restoration mechanism in many β-Ti alloys [2-4]. In this work, with increasing strain, the dislocation density rises rapidly, so that annihilation and rearrangement of dislocations readily occurs resulting in the formation of subgrains. Already at a strain of about 0.02, the rates of work hardening, DRV and CDRX reach a dynamic equilibrium [8, 13].

Flow softening behavior was observed below T_β, and the relative magnitude of the stress drop amounted about 56% and 45% for deformation at 750°C and 800°C, respectively. The softening behavior observed in Ti55531 and Ti7333 with a lower stress drop of about 30%, took place at higher strain rates ($> 10^{-1}$ s^{-1}) [4, 21]. It was attributed to the microstructure that evolves during inhomogeneous deformation because of flow localization (flow instability) at high strain rates due to the relatively low thermal conductivity. Because of the lower strain rate (10^{-2} s^{-1}) used here, the effect of flow instability is deminished. Apparently, the greater stress drop observed in the present work exists for other reasons.

As mentioned in the experimental section, the metastable β-Ti alloy Ti5321 has gone through hot-deformation (bar-rolling) in the ($\alpha+\beta$)-phase field and recrystallization at 900°C. During preheating at high temperature (2 min at 750°C, 800°C and 830°C) in the ($\alpha+\beta$)-phase field lamellar α already precipitates within the β-matrix [1]. As α/β-interphase boundaries are incoherent, some α-phase also heterogeneously nucleates at β grain boundaries leading to a more or less continuous α layer along β grain boundaries. According to Fig. 9 preheating at the deformation temperatures was not long enough to get phase equilibrium. Thus, during deformation (max. duration 1.3 min) α-precipitation continued, but not in lamellar form as evidenced by Fig. 9.

The microstructure evolution during hot-compression (Fig. 9) and quantitative analysis (Fig. 10) suggest that dynamic globularization of the lamellar α-phase existing before deformation has taken place. Based on the study of near β-Ti alloy Ti–5Al–2Sn–2Zr–4Mo–4Cr, Li et al. [35] proposed the following mechanism of dynamic globularization of α-phase lamellae, see also overview by Semiatin [36]. During

hot-compression both phases of the α/β composite with lamellar α-microstructure deform plastically by dislocation slip. α-lamellae preferentially aligned close to CA, i.e. with c-axis almost normal to CA, tend to kink. Because of DRV in the α-lamellae dislocations may arrange themselves into LAGBs aligned normal to the α/β-interphase boundaries. With increasing strain the LAGBs are transformed into HAGBs. Finally, as mechanical equilibrium of interface tensions is not fulfilled, the HAGBs within the α-lamellae lead to interface-tension-driven penetration of the α-plates by the β-phase. With increasing strain the separated α-grains slightly coarsen and become more equiaxed (Fig. 10). The dynamic fragmentation of the α-phase is controlled by bulk diffusion through the β-matrix. The time to complete penetration depends on the diffusivity of the rate controlling solute, the ratio of interface energies of α/α grain boundaries and α/β interphase boundary, and the thickness of the α-lamellae.

While flow softening is not common in metastable β-titanium alloys, it is frequently reported for hot-compression of α/β titanium alloys already containing lamellar/colony α before deformation [36]. Semiatin et al. claim that for Ti64 the noticeable flow softening behavior is not due to dynamic globularization, because a critical true strain of about 0.5 - 1.5 is required for the initiation of dynamic globularization, while noticeable flow softening is already observed at lower true strains of 0.05 - 0.50 [36]. Similarly, as seen in Fig. 1, the majority of the flow softening in this work occurs at compressive strains smaller than about 40%. After a strain of 40%, equiaxed α-grains in β-grains and discontinuous α layers along β-grain boundaries as well as a few β-subgrains/grains are seen in Fig. 9b. Therefore, flow softening observed for Ti5321 may be related to dynamic globularization of α-plates by this

reducing their obstacle effect for dislocation motion in the softer β-phase. A similar intense flow softening observed in Ti1023 [20] was also attributed to the break-up of Widmanstätten platelets during isothermal forging. In addition, the formation of DRX β-grains was considered to significantly contribute to flow softening. However, very fine DRX β-grains are rarely seen in the sample hot-compressed at 750°C to a strain of 40% (Fig. 10a). Even for hot-compression at 800°C to a strain of 80% the volume fraction recrystallized is only 4% (Fig. 6). Moreover, the stress drop during deformation at 750°C (56%) is bigger than that at 800°C (45%). Therefore, the intense flow softening cannot be related to the formation of DRX β-grains. However, as mentioned in section 4.1, DRX at 750°C for true strains larger than 1.0 may be responsible for additional slight flow softening which may be due to grain/interphase boundary sliding. Further microstructural studies with higher resolution at subtransus temperatures and strains lower than 40% are definitely necessary to support the explanation given for the intense flow softening observed for Ti5321.

5. Conclusions

The effect of temperature and strain on the deformation and recrystallization behavior of a hot-compressed metastable Ti-5Al-3V-Mo-2Cr-2Zr-1Nb-1Fe alloy was detaily studied by EBSD. Based on the results the following main conclusions can be drawn:

1. During hot-compression the microstructure evolution with strain is mainly determined by CDRX. Below T_β the preexisting lamellar α-phase microstructure breaks down during deformation and a globular $\alpha+\beta$ dual phase microstructure is formed. The dynamic

globularization influences the CDRX process of the β-phase and leads to flow softening.

2. The texture developing during hot-compression is a <100> <111> double fiber texture with <100> dominating. Both fibers are due to deformation by dislocation slip and DRV leading to CDRX. Above T_β grain boundary bulging into <111> oriented grains increases the intensity of the <100>-fiber on the cost of <111>.

3. During hot-compression below T_β flow softening due to dynamic globularization of α-plates takes place by this reducing their obstacle effect for dislocation motion in the softer β-phase. This process leads to a steady state flow behavior.

Data availability

The data that support the findings of this study are available from the corresponding author upon reasonable request.

References

[1]   G. Lütjering, J.C. Williams, Titanium, 2nd ed., Springer, Berlin, 2007.

[2]   N.G. Jones, R.J. Dashwood, D. Dye, M. Jackson, Thermomechanical processing of Ti–5Al–5Mo–5V–3Cr, Mater. Sci. Eng. A 490 (2008) 369-377.

[3]   J. Zhao, J. Zhong, F.Yan, F. Chai, M. Dargusch, Deformation behaviour and mechanisms during hot compression at supertransus temperatures in Ti-10V-2Fe-3Al, J.

Alloys Compd. 710 (2017) 616-627.

[4]   F. Warchomicka, C. Poletti, M. Stockinger, Study of the hot deformation behaviour in Ti–5Al–5Mo–5V–3Cr–1Zr, Mater. Sci. Eng. A 528 (2011) 8277-8285.

[5]   X.G. Fan, Y. Zhang, P.F. Gao, Z.N. Lei, M. Zhan, Deformation behavior and microstructure evolution during hot working of a coarse-grained Ti-5Al-5Mo-5V-3Cr-1Zr titanium alloy in beta phase field, Mater. Sci. Eng. A 694 (2017) 24-32.

[6]   H. Matsumoto, M. Kitamura, Y.P. Li, Y. Koizumi, A. Chiba, Hot forging characteristic of Ti–5Al–5V–5Mo–3Cr alloy with single metastable β microstructure, Mater. Sci. Eng. A 611(2014)337–344.

[7]   H.J. McQueen, Development of dynamic recrystallization theory, Mater. Sci. Eng. A 387-389 (2004) 203-208.

[8]   T. Sakai, A. Belyakov, R. Kaibyshev, H. Miura, J.J. Jonas, Dynamic and post-dynamic recrystallization under hot, cold and severe plastic deformation conditions, Prog. Mater. Sci. 60 (2014) 130-207.

[9]   D.G. Cram, H.S. Zurob, Y.J.M. Brechet, C.R. Hutchinson, Modelling discontinuous dynamic recrystallization using a physically based model for nucleation, Acta Mater. 57 (2009) 5218-5228.

[10]   M. Hasegawa, M. Yamamoto, H. Fukutomi, Formation mechanism of texture during dynamic recrystallization in γ-TiAl, nickel and copper examined by microstructure observation and grain boundary analysis based on local orientation measurements, Acta Mater. 51 (2003) 3939-3950.

[11] J. K. Solberg, H.J. McQueen, N. Ryum, E. Nes, Influence of ultra-high strains at elevated temperatures on the microstructure of aluminium, Part I, Phil. Mag. A, 60 (1989) 447-471.

[12] S. Gourdet, F. Montheillet, A model of continuous dynamic recrystallization, Acta Mater. 51 (2003) 2685-2699.

[13] F.J. Humphreys, M. Hatherly, Recrystallization and Related Annealing Phenomena, 2nd ed., Elsevier, Oxford, 2004.

[14] M. Dikovits, C. Poletti, and F. Warchomicka, Deformation mechanisms in the near-β Titanium Alloy Ti-55531, Met. Mater. Trans. A, 45 (2014) 1586-1596.

[15] B. Sander, D. Raabe, Texture inhomogeneity in a Ti-Nb-based β-titanium alloy after warm rolling and recrystallization, Mater. Sci. Eng. A 479 (2008) 236-247.

[16] N.P. Gurao, S. Suwas, Study of texture evolution in metastable β-Ti alloy as a function of strain path and its effect on α transformation texture, Mater. Sci. Eng. A 504 (2009) 24-35.

[17] M. Premkumar, V.S. Himabindu, S. Banumathy, A. Bhattacharjee, A.K. Singh, Effect of mode of deformation by rolling on texture evolution and yield locus anisotropy in a multifunctional β titanium alloy, Mater. Sci. Eng. A 552 (2012) 15-23.

[18] S. Banumathy, R.K. Mandal, A.K. Singh, Texture and anisotropy of a hot rolled Ti–16Nb alloy, J. Alloys Compd. 500 (2010) L26-L30.

[19] B. Gu, P. Chekhonin, R. Schaarschuch, C.-G. Oertel, S.W. Xin, C.L. Ma, L. Zhou, W.M. Gan, W. Skrotzki, Microstructure, texture and hardness of a metastable β-titanium alloy after bar-rolling and annealing, J. Alloys Compd. 825 (2020) 154082.

[20] M. Jackson, N.G. Jones, D. Dye, R.J. Dashwood, Effect of initial microstructure on plastic flow behaviour during isothermal forging of Ti–10V–2Fe–3Al, Mater. Sci. Eng. A 501 (2009) 248-254.

[21] J.K. Fan, H.C. Kou, M.J. Lai, B.Tang, H. Chang, J.S. Li, Hot deformation mechanism and microstructure evolution of a new near β titanium alloy, Mater. Sci. Eng. A 584 (2013) 121-132.

[22] A. Samiee, G. Casillas, M. Ahmed, D.G. Savvakin, R. Naseri and E. Pereloma, Formation of deformation-induced products in a metastable β-titanium alloy during high temperature compression. Metals 8 (2018) 100.

[23] Y.Q. Zhao, C.L Ma, H. Chang, S.W. Xin, L. Zhou, New high strength and high toughness titanium alloy with 1200 MPa, Mater. China, 35 (2016) 914-918. (In Chinese)

[24] S.I. Wright, M.M. Nowell, D.P. Field, A review of strain analysis using electron backscatter diffraction, Microsc. Microanal. 17 (2011) 316-329.

[25] K. Li, P. Yang, The formation of strong {100} texture by dynamic strain-induced boundary migration in hot compressed Ti-5Al-5Mo-5V-1Cr-1Fe Alloy, Metals 7 (2017) 412.

[26] F. Cruz-Gandarilla, R.E. Bolmaro, H.F. Mendoza-Leon, A.M. Salcedo-Garrido, J.G. Cabanas-Moreno, Study of recovery and first recrystallisation kinetics in CGO Fe3%Si steels using misorientation-derived parameters (EBSD), J. Microscopy 275 (2019) 133-148.

[27] J. Rasti, A. Najafizadeh, M. Meratian, Correcting the stress-strain curve in hot

compression test using finite element analysis and Taguchi method, Int. J. ISSI 8 (2011) 26-33.

[28] A.A. Gazder, M. Sanchez-Araiza, J.J. Jonas, E.V. Pereloma, Evolution of recrystallization texture in a 0.78 wt.% Cr extra-low-carbon steel after warm and cold rolling, Acta Mater. 59 (2011) 4847-4865.

[29] L.S. Toth, Y. Estrin, R. Lapovok, C. Gu, A model of grain fragmentation based on lattice curvature, Acta Mater. 58 (2010) 1782-1794.

[30] W.F. Hosford, Mechanical Behavior of Materials, 2nd ed., Cambridge University Press (2010).

[31] O. Engler, V. Randle, Introduction to Texture Analysis: Macrotexture, Microtexture, and Orientation Mapping, 2nd ed., CRC Press, Taylor & Francis Group, Boca Raton, 2010.

[32] S. Primig, H. Leitner, W. Knabl, A. Lorich, H. Clemens, R. Stickler, Textural evolution during dynamic recovery and static recrystallization of molybdenum, Metall. Mater. Trans. A 43 (2012), 4794-4805.

[33] C.S. Barrett, T.B. Massalski, Structure of metals, McGraw-Hill, New York, 1966.

[34] L. Meng, T. Kitashima, T. Tsuchiyama, M. Watanabe, β-Texture evolution during a precipitation in the two-step forging process of a near-β titanium alloy, Metall. Mater. Trans. A (2020) 51A, 5112-5122.

[35] L. Li, J. Luo, J.J. Yan, M.Q. Li, Dynamic globularization and restoration mechanism of Ti–5Al–2Sn–2Zr–4Mo–4Cr alloy during isothermal compression, J. Alloys Compd. 622 (2015) 174-183.

[36]   S.L. Semiatin, An overview of the thermomechanical processing of α/β titanium alloys: current status and future research opportunities, Metall. Mater. Trans. A 51 (2020) 2593-2625.